

Article

Structural Hierarchy of PA6 Macromolecules after Hydrostatic Extrusion

Monika Skorupska ^{1,*}, Mariusz Kulczyk ¹, Piotr Denis ², Dominik Grzęda ³, Anna Czajka ³
and Joanna Ryszkowska ³

¹ Institute of High Pressure Physics, Polish Academy of Sciences (Unipress), Sokołowska 29, 01-142 Warsaw, Poland; mariusz@unipress.waw.pl

² Institute of Fundamental Technological Research, Polish Academy of Sciences, Pawinskiego 5B, 02-106 Warsaw, Poland; pdenis@ippt.pan.pl

³ Faculty of Materials Science and Engineering, Warsaw University of Technology, Ul. Wołoska 141, 02-507 Warsaw, Poland; dominik.grzeda.dokt@pw.edu.pl (D.G.); anna.czajka2.dokt@pw.edu.pl (A.C.); joanna.ryszkowska@pw.edu.pl (J.R.)

* Correspondence: monikaw@unipress.waw.pl

Abstract: This article presents the influence of severe plastic deformation by hydrostatic extrusion (HE) on the thermal and structural properties of polyamide 6 (PA6). During the hydrostatic extrusion process, a fibrous structure oriented along the extrusion direction is formed, which was visualized during microscopic observations. The degree of crystallinity was analyzed by differential scanning calorimetry (DSC). Wide-angle X-ray scattering diffraction (WAXS) analysis was used to partially characterize the PA6 structure after the HE process. The contents of various forms of the crystalline phase in PA6 samples before and after the HE process were analyzed in fragments of spectroscopy in infrared (FTIR). The favorable properties of PA6 after the HE process were obtained after deformation under conditions generating an adiabatic temperature higher than the glass transition temperature and lower than the temperature of the onset of melting of the crystalline phase. Thermal analysis using DSC allowed us to conclude that in the PA6 after the HE process generating deformations in the range of 0.68–1.56, the proportion of the crystalline phase α increases in PA6. As the deformation increases in the HE process, the crystalline phase proportion increases by 12% compared to the initial material (before HE). The glass transition temperature of PA6 is ca. 50.6 °C, reduced for the sample after the HE process at a small deformation of 0.68 (PA6_0.68) to ca. 44.2 °C. For other samples, T_g is ca. 53.2–53.5 °C. As a result of the analysis of WAXS diffractograms of PA6 samples after various deformations in the HE process, the presence of typical peaks of phases α_1 and α_2 and γ was observed. The results of the FTIR spectroscopic analysis confirm these observations that as the deformation increases, the proportion of the crystalline phase α increases.

Keywords: hydrostatic extrusion; polyamide 6; structure; thermal properties



Citation: Skorupska, M.; Kulczyk, M.; Denis, P.; Grzęda, D.; Czajka, A.; Ryszkowska, J. Structural Hierarchy of PA6 Macromolecules after Hydrostatic Extrusion. *Materials* **2023**, *16*, 3435. <https://doi.org/10.3390/ma16093435>

Academic Editor: Cristina Della Pina

Received: 13 March 2023

Revised: 24 April 2023

Accepted: 26 April 2023

Published: 28 April 2023



Copyright: © 2023 by the authors. Licensee MDPI, Basel, Switzerland. This article is an open access article distributed under the terms and conditions of the Creative Commons Attribution (CC BY) license (<https://creativecommons.org/licenses/by/4.0/>).

1. Introduction

Polyamide 6 is a popular synthetic polymer widely used industrially and with many applications in engineering, including medicine. They are partially crystalline thermoplastics [1]. One of the methods of modifying PA6 to increase its strength properties is processing in the hydrostatic extrusion (HE) process.

The effectiveness of this method in terms of the increase in the materials' strength has been demonstrated to date for metals and metal alloys in many publications [2–7]. The HE processing of polymers was first described in 1964 [8]. One of the first papers showing the hydrostatic extrusion of Nylon 6 was published in 1978 [9]. The authors focused on the study of distortion grids and the influence of extrusion pressure on the polymer structure. Extensive data on hydrostatic extrusion parameters and properties of polymers after deformation processes were collected in the chapter “Polymers” of the book

by N. Inoue [10]. The description of the HE process and the impact of its parameters on the strength properties of PA6 are presented in the paper by M. Skorupska et al. [11].

The hydrostatic extrusion process has been shown to increase strength properties such as tensile modulus, which rose by about 65%, and tensile strength, which rose by almost 500%. The changes in the tensile path observed are typical of changes caused by the stretching of polymers with increased pressure in the measuring chamber [12].

Based on the presented results, it can be concluded that the higher the strain applied during the HE process, the greater the tensile strength (σ_M) of the PA6 after the HE process. The tensile strength changes (σ_M) of the PA6 can be associated with changes in the structure of PA6 after the HE process, as indicated by the results of the studies presented by Li et al. [13].

The type of crystalline phase is most often described using wide-angle X-ray scattering (WAXS) [14–21]. In the form of α , the amide group and group $(CH_2)_5$ planes are parallel to each other, whereas in the form of γ , they are approximately perpendicular. Phase α is thermodynamically the most stable crystalline form [13]. The form γ can be converted into α by melting and then recrystallization, [22] by annealing at 160 °C in a saturated vapor atmosphere without any significant loss of orientation [23] and by applying stresses at room temperature. Intermediate crystalline forms occur between these phases [21,24–35].

Several methods are used to describe the degree of crystallinity of PA6—differential scanning calorimetry (DSC), density measurements, X-ray scattering, infrared and Raman spectroscopy, and nuclear magnetic resonance [36]. The determination of the degree of crystallinity allows us to understand the changes in the properties of PA6 after the thermo-mechanical processing process. Most often, DSC is used for this purpose. However, during the measurement in the annealing process, there is a rearrangement in the unstable crystalline phases, which causes the melting endotherm to contain thermal effects derived from the melting of the stable and unstable phases. Therefore, DSC research is complemented by other analysis techniques. Observation methods such as scanning electron microscopy (SEM) and polarized optical microscopy (POM) are also used to describe the structure.

To explain the reasons for the changes in the strength properties of PA6 after the HE process, the changes in the structure of these materials were analyzed. The results presented in the study by Skorupska et al. [11] indicate that the structure of PA6 changes after the HE process. Based on the SEM images presented in this study [11], it was found that during the HE process, a fibrous structure is formed with fibers arranged along the direction of extrusion in the HE process. To confirm these observations, microscopic observations were made using SEM and POM.

The impact of cold HE process parameters on changes in the structure of PA6 processed by this method was analyzed.

2. Materials and Methods

2.1. Material and Processing

The unmodified extruded polyamide 6 was purchased in the form of a rod with a diameter of 15.6 mm from MEGA-TECH s.c., Grodzisk Mazowiecki, Poland [37].

Samples of unmodified PA6 were subjected to the HE processes described in Table 1. Hydrostatic Extrusion was performed at a press designed and manufactured at the Institute of High Pressure Physics of the Polish Academy of Sciences (Warsaw, Poland). The press with a working chamber of 22 mm enables extrusion at pressures of up to 2 GPa. Prior to the HE processes, the rods were coated with a silicone-oil-based grease and squeezed out at a linear speed (v) in the range of 3.5–111 mm s⁻¹ through forming a matrix with (die) the vertex angle $2\alpha = 45^\circ$ and diameters of 6, 7 and 8 mm.

The samples were subjected to true strain in the range of 0.68–1.90. The pressure values in the HE process were in the range of 100–430 MPa, which translated into the generation of heat in the material described by the adiabatic temperature in the range of 50–211 °C. All samples were extruded at the same extrusion rate of 5 mm s⁻¹.

Table 1. Initial mechanical properties of the PA6 polyamide.

Series	True Strain, ϵ	Linear Speed V (mm·s ⁻¹)	Extrusion Pressure p (MPa)	Adiabatic Temperature T_{ad} (°C)
PA6	0	0	0	20
PA6_0.68	0.68	5	103	50
PA6_1.25	1.25	5	180	88
PA6_1.56	1.56	5	262	128
PA6_1.90	1.90	5	430	211

2.2. Experimental

2.2.1. Tensile Test

The static tensile test (Zwick/Roell Z250, Ulm, Germany) was performed for samples with a diameter of 5 mm and a length of 10 mm at a tensile speed of 1 mm·min⁻¹.

2.2.2. WAXS

WAXS experiments were carried out using a Bruker D8 (Bruker, Karlsruhe, Germany) Discover diffractometer operating at 1.6 kW nominal power with the Cu radiation source (wavelength 1.5418 Å). Data were recorded at room temperature, using a Bruker AXS Lynxeye 1-D detector (Bruker, Karlsruhe, Germany), in reflective mode. On the primary (source) side, a parallel Goebel-mirror optic was used, with a 1.2 mm linear slit and a 1 mm spot collimator. On the secondary (detector) side, a 2.5° divergence soller-slit was used.

2.2.3. DSC

DSC analysis of PA6 was performed using a differential scanning calorimeter DSC Q1000 (TA Instruments, New Castle, DE, USA). Samples (ca. 7 mg) were closed in hermetic aluminum cups and heated and cooled at 10 °C min⁻¹ in the temperature range 0 to 250. Based on the DSC thermograms obtained, melting peak distributions were performed using Origin Pro 8 and Fit Multi-peaks with Gaussian distribution. The crystalline weight fraction was computed from the enthalpy of the melting endotherm using the melting enthalpy of 100% crystallized $\Delta H_m 0(\text{PA6}) = 230 \text{ J/g}$ [36] whatever the crystalline form.

2.2.4. FTIR

PA6 samples were analyzed using absorption spectra obtained with a Nicolet 6700 spectrophotometer (Thermo Electron Corporation, Waltham, MA, USA) equipped with an attenuated total reflection (ATR) module. Each sample was scanned 64 times in the wavelength range of 4000–400 cm⁻¹. The results were analyzed with the Omnic Spectra 8.2.0 software (Thermo Fisher Scientific Inc., Waltham, MA, USA). For each PA6 sample, a representation of three spectra was taken. The analysis of the spectra using OMNIC was carried out using the Gaussian distribution, assuming a linear baseline. Phase α and γ participation was calculated using the dependencies formulated by Dechant [38], for the crystalline variety α from Formula (1) and for the crystallographic variety γ :

$$X_{IR\alpha} = \frac{A_{1030}}{A_{1075}} \quad (1)$$

$$X_{IR\gamma} = \frac{A_{975}}{A_{1075}} \quad (2)$$

where: $X_{IR\alpha}$ and $X_{IR\gamma}$ describe the proportion of polymorphic varieties of PA6 ordered regions, and A_{974} , A_{1030} and A_{1073} are the fields of band absorbance at a wave number of 974 cm⁻¹, 1030 cm⁻¹ and 1075 cm⁻¹, respectively.

2.2.5. POM

Scrapings were cut from polyamide samples in the longitudinal orientation and crosswise to the direction of hydrostatic extrusion. The scrapings obtained by cutting were transferred to a basic microscope slide with a drop of immersion oil and covered with a flat cover slip. The cutting of the scrapings was performed with the use of a Leica EM FC6 ultramicrotome (Leica Microsystems, Wetzlar, Germany), using the following cutting parameters: feed speed— 0.40 mm s^{-1} , slice thickness— 2400 nm , room temperature. The slices were cut with glass knives. Observation of the samples was carried out using a Biolar P1 polarization–interference microscope (PZO, Warszawa, Poland), using a 20X objective and crossed polaroids, also at room temperature. Observations were carried out in dark and bright fields. The parameter of spherulites and fibers present in a polarized optical microscopy (POM) image was quantified using ImageJ (Fiji ImageJ 2.9.0).

2.2.6. SEM

Using a ZEISS SEM microscope (ZEISS, Jena, Germany), model ULTRA PLUS with a Gemini column (Jena, Germany), structural analysis was performed. Samples were frozen in liquid nitrogen for 5 min and then fractured by bending. The surface of these cracks was observed. The samples were dusted with a layer of gold before observation.

3. Results and Discussion

The HE process of polyamide 6 was carried out at different sample deformations in the range of 0.68–1.90 resulting in an extrusion pressure in the range of 100–450 MPa. Hydrostatic extrusion was carried out at the same linear deformation rate of 5 mm min^{-1} . The HE process at 430 MPa was an unstable process, resulting in changes in the strength properties of PA6_1.90 samples not being analyzed.

3.1. Mechanical Properties of PA6 after Cold HE

As a result of the research on strength properties, some of which are presented in the study by Skorupska et al. [11], it was found that during the stretching of the example samples subjected to the HE process, the nature of the tensile curves changed (Figure 1).

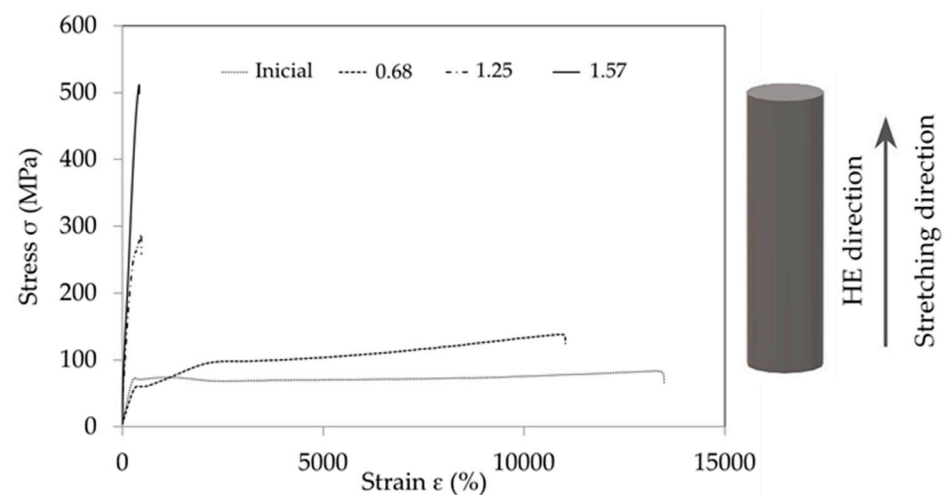


Figure 1. Examples of tensile curves before hydrostatic extrusion (Inical) and after the process at different true strains ($\epsilon = 0.68$, $\epsilon = 1.25$, $\epsilon = 1.57$).

The tensile PA6 samples are described by the tensile curve typical of materials in the viscous elastic state, as is the PA6_0.68 sample. In contrast, samples PA6_1.25 and PA6_1.56 are described by tensile curves typical of materials in a brittle elastic state, also called vitreous.

The observed changes in the tensile curves are typical of changes caused by the stretching of polymers at increased pressure in the measuring chamber [12]. Based on the results presented in Figure 1, it can be concluded that the higher the deformation in the HE process, the greater the modulus of elasticity of PA6 after the HE process. Changes in the modulus of elasticity of PA6 can be associated with changes in the morphology of PA6 after the HE process, as indicated by the results of the research presented by Li et al. [13]. Based on the research presented in this study, it was found that the modulus of elasticity of PA6 in the form of α is more than twice as high as for PA6 in the form γ .

3.2. Structural Investigations

After the hydrostatic extrusion process, polyamide PA6 crystallizes. During crystallization, spherulites are formed from the lamellae [13]. Images of the sample fracture structure made across the extrusion direction (PA6 across) and along the HE direction (PA6 along) are shown in Figure 2.

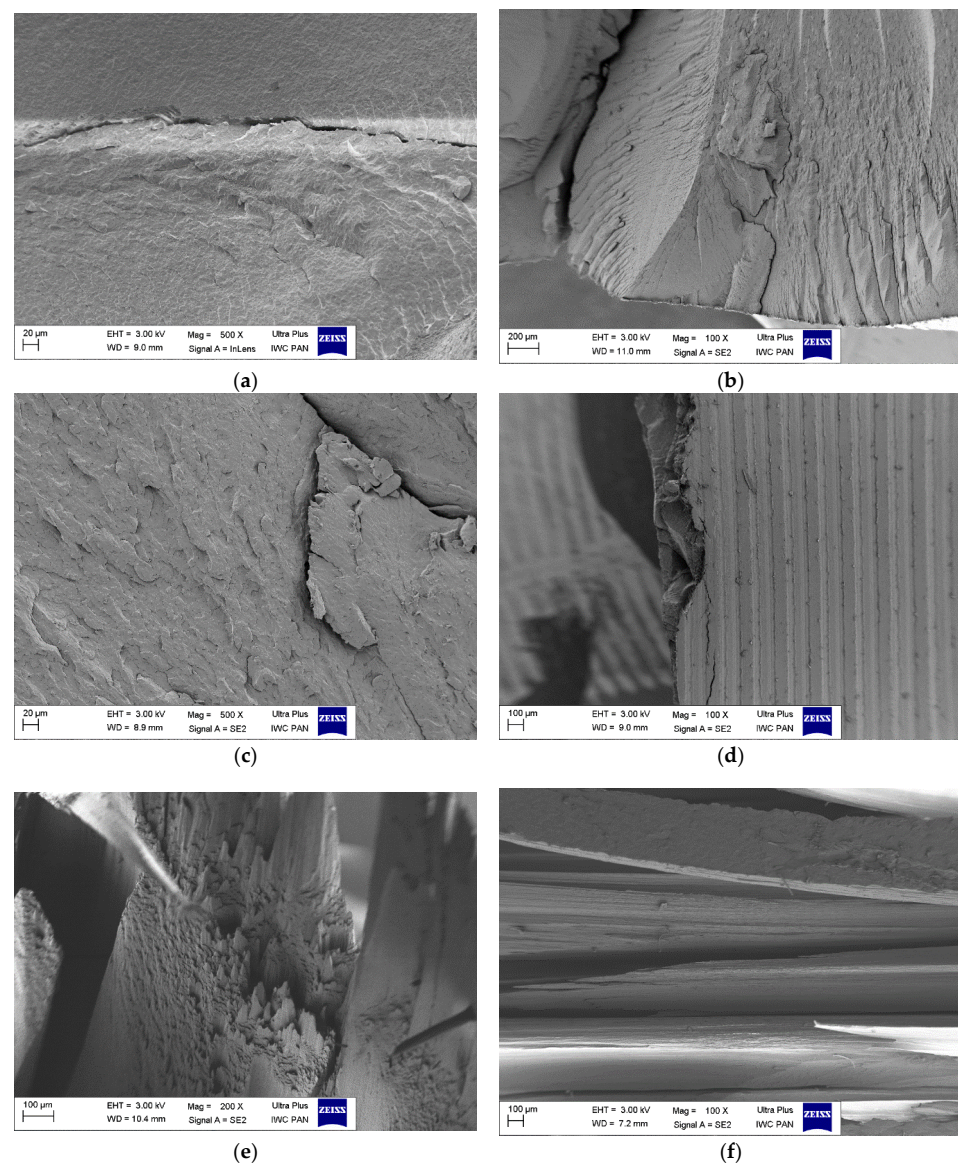


Figure 2. Scanning electron microscopy (SEM) images of cryo-fractured transverse cross-sections of the polyamide PA6 in initial state: PA6_across (a), PA6_along (b). Rod after cold hydrostatic extrusion HE with true strain $\varepsilon = 0.68$: PA6_0.68_across (c), PA6_0.68_along (d) and rod after cold HE with $\varepsilon = 1.57$: PA6_1.56_across (e), PA6_1.56_along (f).

The sizes of these ovals are less than 20 μm . It follows from the results presented by Osorio et al. [39] that the size of spherulites in the PA6 samples they studied varied in the range of 10–20 μm .

The PA6_0.68_across fracture is different from the PA6_across fracture. The elements of the surface structure of this fracture have the character of oval islands with elongated shapes. On the other hand, at the fracture of this sample along the HE direction (PA6_0.68_along), elements in the form of bands arranged parallel to each other are visible, these bands differ in width, and the narrower bands have a width of approx. 50 μm , and the wider ones of ca. 80 μm . They are separated by a band with a width of 40–60 μm . It can be assumed that these bands were formed by straightened-out fragments of lamellae forming spherulitic structures from different varieties of the PA6 crystal phase (α and γ). The structure of the PA6_1.56 sample fractures is different. The band structures formed in this material are characterized by such high strength that it was impossible to perform a flat fracture in the across direction to the HE direction. The PA6_1.56_across sample fractures allow broken and pulled fiber bundles to be observed. At the fracture formed along the HE direction (PA6_1.56_along), wide fiber bundles of 140–180 μm are visible, as well as narrow bundles with a much smaller size of ca. 60–80 μm , which are separated by gaps of approx. 60 μm . As in the case of the PA6_0.68_along material, the band structures were formed in this material. They are formed from straightened fragments of spherulite lamellae of different varieties of the PA6 crystalline phase (α and γ). Higher pressure during the HE process at deformation $\varepsilon = 1.56$ caused more agglomerates of bands connected by hydrogen bonds to form than in the material under deformation $\varepsilon = 0.68$.

Analysis of sample fracture images indicates that an increase in true strain during the HE process results in an increase in the cross-sectional diameter of the fiber bundles formed during the HE process. This change in the structure of the materials is probably the reason for the significant increase in the strength of PA6 after the HE process.

Observations of ultramicrotome cuttings were also made with a polarized scanning transmission electron microscope; exemplary images are shown in Figure 3.

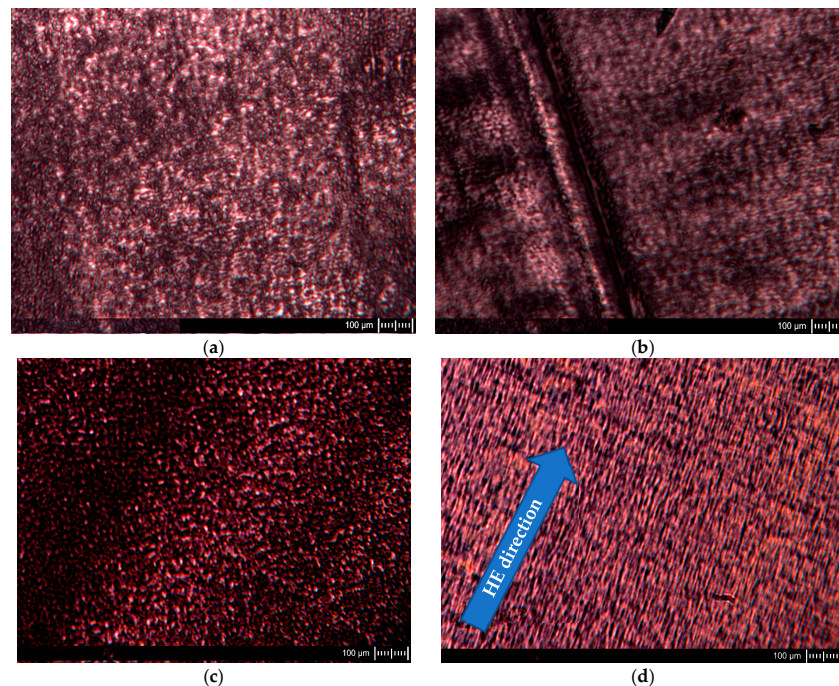


Figure 3. Example images of POM sample cuttings before (a,b) and after HE process (c,d). The samples labeled across: (a,c) were made across the extrusion direction for PA6 and across the HE direction for samples after this process, and the samples labeled (b,d) along the extrusion direction for PA6 and along the HE direction for samples after this process.

The images of the PA6 sample cuttings at baseline observed in POM show oval-shaped structural elements reflecting the shape of the spherulites formed in these samples. A similar pattern was observed for the sample in the case of a cut made across the extrusion direction as well as along the extrusion direction. The images of PA6_1.56_across sample cuts made across the HE direction are similar to the PA6 sample cutting images. Images of the structure of the sample PA6_1.56_along cut made along the HE direction differ significantly from that made across the HE direction. The structural elements of the cuts made along the HE direction have the shape of rods arranged in a regular manner parallel to each other. Based on the SEM and POM images, a scheme of changes in the structure of PA6 caused by deformation in the HE process is proposed, which is presented in the diagram shown in Figure 4.

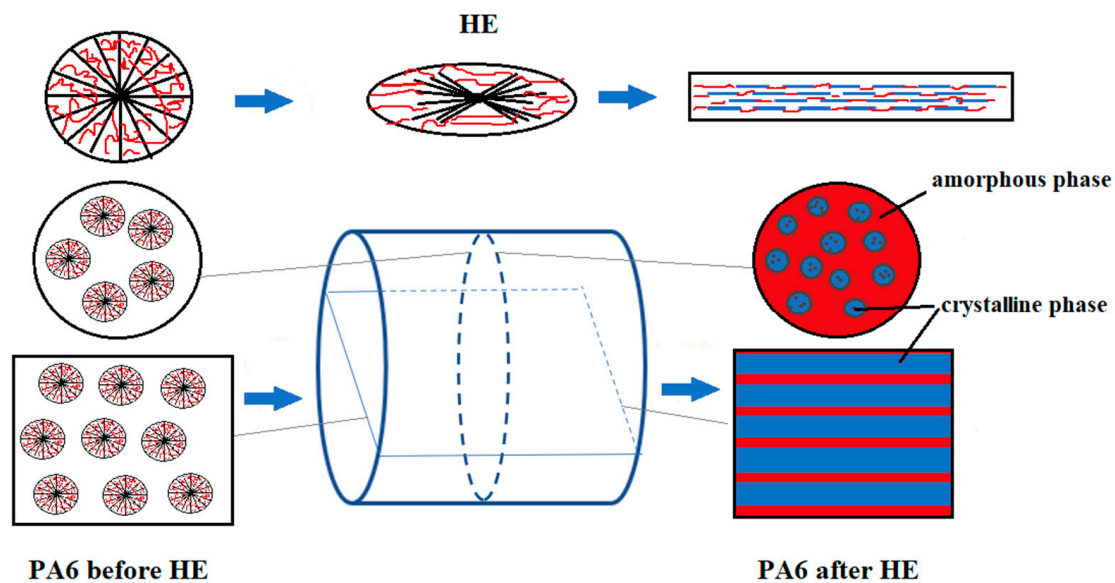


Figure 4. Diagram of changes in the structure of PA6 sample fractures before and after the HE process.

During the HE process, the deformation of partially crystalline polymers in the solid state occurs. This process is possible at a temperature above the glass transition temperature (T_g) and below the melting point (T_m). During deformation in this temperature range, cavitation phenomena [40] and phenomena resulting from crystal plasticity can occur, causing crystallite regrouping [41,42]. In the HE process, the optimal parameters of the extrusion process are achieved below T_m , and, therefore, it can be assumed that the course of the deformation process depends on the degree of crystallization of the processed material since crystalline areas limit the movement of molecules [43] and may also be the reason for the strengthening of materials due to the orientation of macromolecules [44].

3.3. Results of Diffraction Analysis

PA6 occurs in two thermodynamically equilibrium crystalline forms α and γ , and one mesomorphic form β [31,45,46]. During slow cooling, the molten state forms phase α , and during rapid melting, phase γ . The formation of the γ phase was also observed in nanocomposites, its nucleation was caused by nanofillants such as clay, zinc oxide and mica [47–50]. In order to characterize the structure of PA6 after the HE process, WAXS diffractograms were performed for selected PA6s before and after the HE process. The cross-sectional surfaces of the samples (across) (Figure 5) and the cross-sectional surfaces made along the extrusion direction (along) (Figure 6) were analyzed. Based on the analysis of the diffractograms, listed in Table 2 are reflections seen in the diffractograms shown in Figure 5, obtained after the HE process at different degrees of deformation.

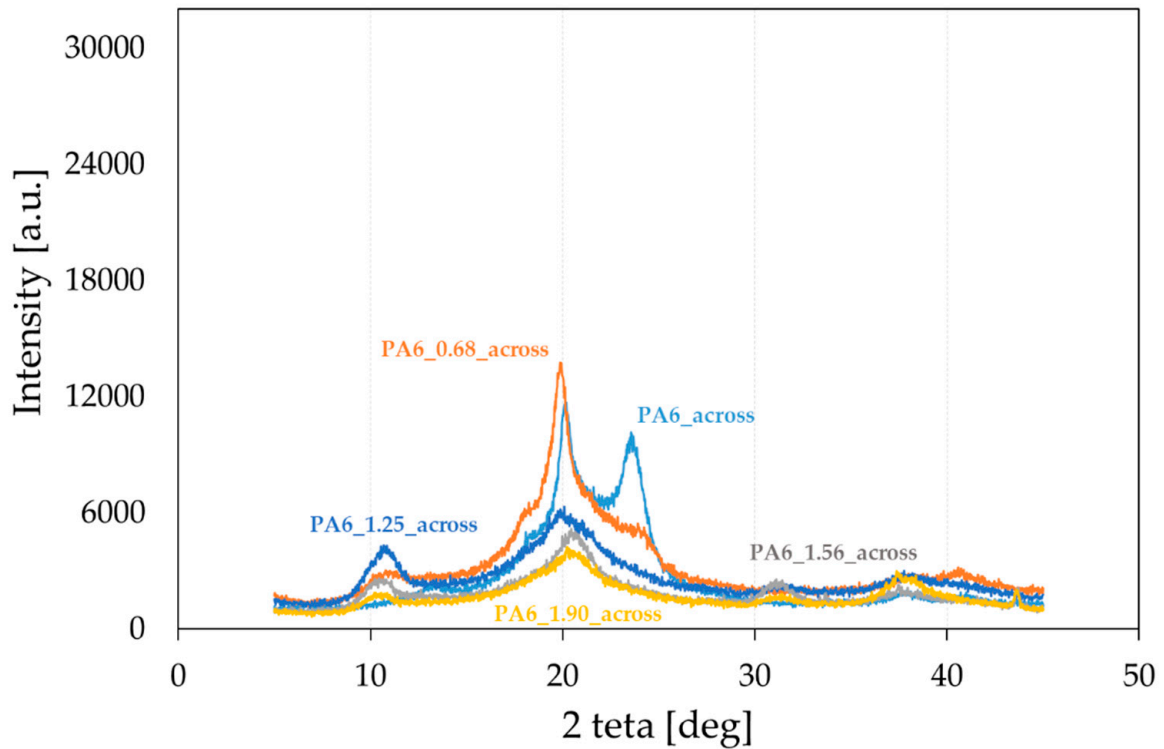


Figure 5. Diffractograms of PA6 samples before the HE process (PA6) and after the HE process at variable true strain. Diffractogram obtained for a cross-sectional sample.

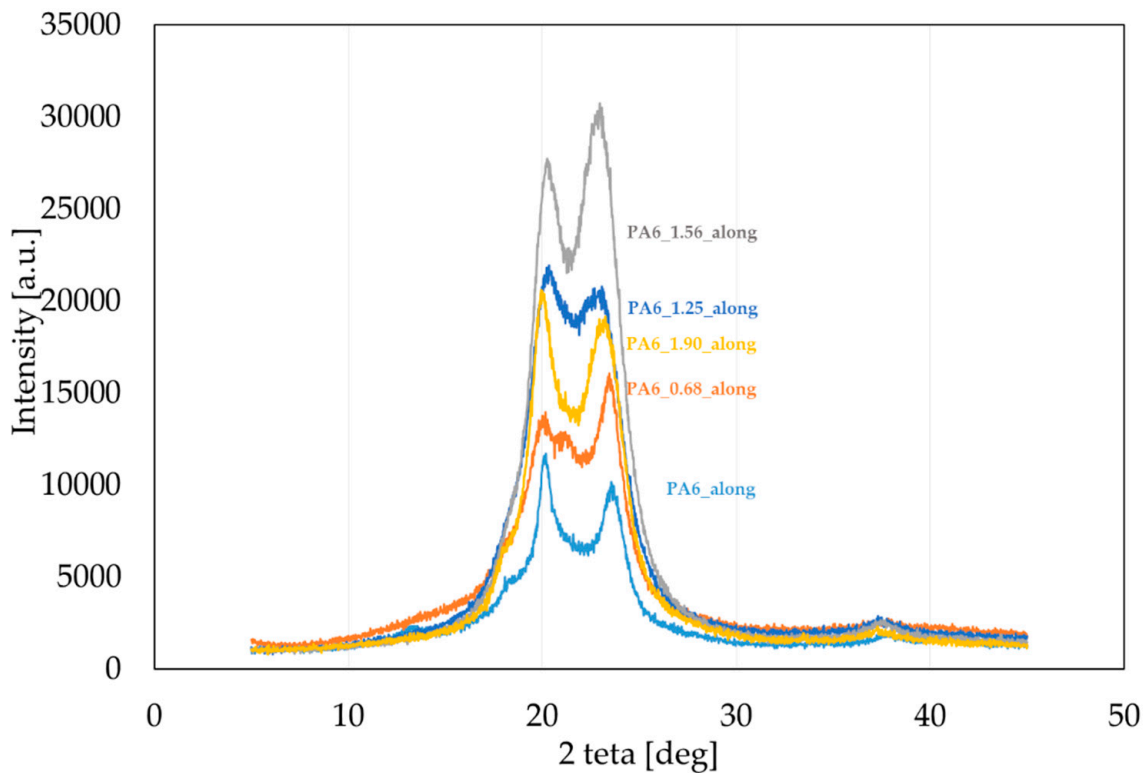


Figure 6. Diffractograms of PA6 samples before the HE process (PA6) and after the HE process at variable true strain. Diffractogram obtained for a sample from a cross-section made along the HE direction.

Table 2. Description of the sample WAXS diffractograms before and after the HE process.

Series	Peak Position [deg.]			
	α_1	α_2	γ	Amorphous
PA6_across	20.01	23.59	21.21	20.90
PA6_0.68_across	19.85	24.07	21.06	20.51
PA6_1.25_across	19.80	-	21.09	20.08
PA6_1.56_across	-	-	20.54	20.27
PA6_1.90_across	20.26	-	20.45	20.21
PA6_along	20.09	23.65	20.56	21.25
PA6_0.68_along	19.89	23.49	21.18	21.19
PA6_1.25_along	20.16	23.24	21.85	21.40
PA6_1.56_along	20.20	23.05	21.88	21.63
PA6_1.90_along	19.95	23.33	20.99	21.61

At room temperature, there can be two phases, α and γ in PA6. According to [16,23,51], the characteristic peaks of the α_1 -phase appear at an angle 2θ between 20.2 and 20.6° ($200, \alpha_1$) and the α_2 -phase at an angle $2\theta = 24^\circ$ ($002 + 202, \alpha_2$). However, for the γ -phase, there are reflections coming from two forms of this phase: at an angle of 21° ($100, \gamma_1$) and 22.5° ($201 + 200, \gamma_2$) [52].

Based on the introduction to the publication [53] and the information contained therein, based largely on the long and intensively studied structure of PA6 in the history of polymer research, it is possible to briefly characterize the phases α and γ :

- α is composed of PA6 extended chains while γ form is composed of pleated chains;
- Mainly intra-sheet hydrogen bonding is present in α form, while in the γ form inter-sheet hydrogen bonds are dominant;
- Young modulus of α form is considered to be higher than γ form (due to differences in ordering of the structures in both forms);
- α form is considered to be more thermodynamically stable.

According to the above characteristics, it can be considered that the main differences between the α and γ forms are the shape of the chains (extended vs. pleated) and the hydrogen bonding direction which results in different crystal structures and d-spacings (hydrogen bondings in pleated γ chains are tilted by about 60° compared to the bonding direction of the α form). We consider that it is relatively safe to assume that mechanical deformations which accompany the extruding process may result in changes in the shape of the chains (it may pleat them or extend them) as well as in the directions of chains.

It was found by analyzing the diffractograms PA6_across and PA6_along that the reflections coming from phase α_1 and α_2 occur at $2\theta = 20.01^\circ$ and 23.49° and $2\theta = 20.09^\circ$ and 23.65° , respectively. The reflection from phase γ occurs at $2\theta = 21.21^\circ$ and $2\theta = 20.56^\circ$, respectively. The peak intensities for the output PA6_across and PA6_along are similar, suggesting that the samples in the initial state are close to isotropic structures. Diffractograms of samples after the HE process made across (Figure 5) and along the HE direction (Figure 6) differ markedly in the intensity of phase-related reflections α_1 and α_2 and γ , which indicates their anisotropic structure.

In the diffractograms of HE-deformed samples taken across the direction of deformation (Figure 5), reflections were observed from phase α_1 at $2\theta = 19.80$ – 20.26° , and this reflection does not occur for the sample PA6_1.56_across only. For the sample PA6_0.68_across, there is also a reflection from phase α_2 at $2\theta = 24.07^\circ$. Reflections from phase γ occur in the range of 20.45 – 21.06° ; the greater the deformation in the HE process, the closer the reflection position is to 20.4° . On the other hand, in diffractograms of the surface of samples after the HE process made along the direction of extrusion (Figure 6), there are peaks coming from phase α_1 at $2\theta = 19.89$ – 20.20° and from phase α_2 at $2\theta = 23.05$ – 23.49° . The reflection from phase α_2 moves towards lower angles at deformations 0.68, 1.25 and 1.56. For phase γ reflections occurring in the range of 20.99 – 21.88° ,

and for samples under deformation 0.68, 1.25 and 1.56, the reflections from this phase move towards angles closer to 22° .

A summary of the results of the analysis of reflections in the obtained diffractograms is presented in Table 2.

The deconvolution of the WAXS spectra is shown in Figure 7. The results of the analysis of the deconvolution into component bands are shown in Table 3.

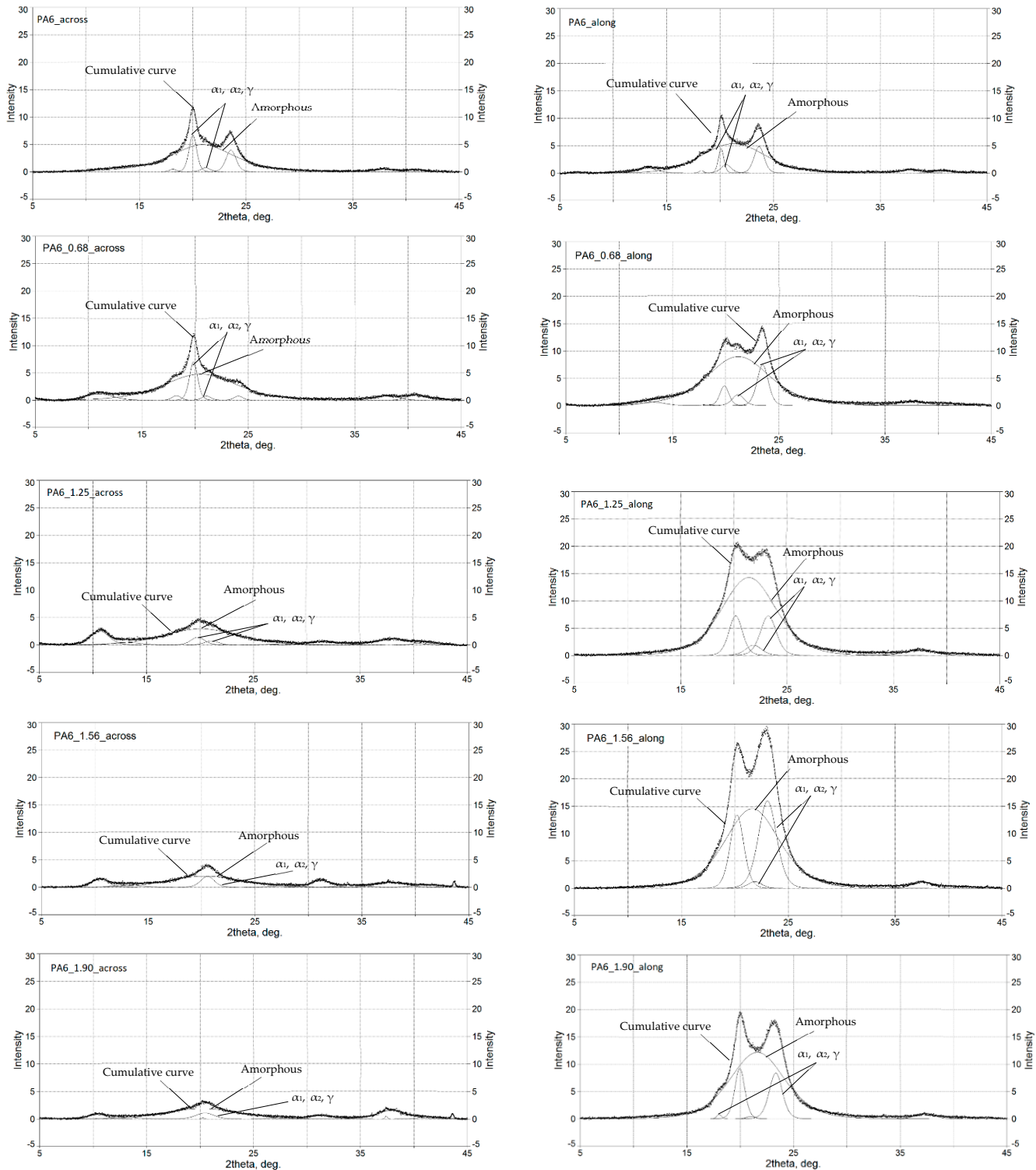


Figure 7. Distribution curves of diffractograms of the tested materials.

Table 3. Description of component bands on WAXS diffractograms of pre-HE and post-HE of the samples.

Series	Arbitrary Units			
	α_1	α_2	γ	Amorphous
PA6_across	6.33	4.87	0.84	42.15
PA6_0.68_across	7.16	0.84	0.89	43.12
PA6_1.25_across	2.36	0	1.22	26.22
PA6_1.56_across	0	0	3.35	17.94
PA6_1.90_across	0.06	0	2.48	16.62
PA6_along	2.96	5.95	1.92	40.80
PA6_0.68_along	4.02	10.38	2.99	72.72
PA6_1.25_along	12.14	14.13	3.71	96.67
PA6_1.56_along	22.36	35.58	2.03	98.43
PA6_1.90_along	11.33	13.54	0.47	82.47

In the longitudinal direction (along the deformation direction):

- For deformations 0.68, 1.25 and 1.56, an increase in the contribution of the alpha phase;
- Components are observed, and therefore an increase in the proportion of longitudinally directed chains (at the same time, a slight increase in the gamma phase component to deformation of 1.25 and then its sharp decline. In quantitative terms, however, the contribution of the gamma phase to the structure is small relative to the alpha phase in this direction, a maximum of about 12% for the 1.25 sample, and only about 3% of the contribution taking into account the amorphous phase);
- The high contribution of the alpha structural component can therefore be reflected in the high rigidity of the material, increasing with deformation up to a value of 1.56 deformation. It can be seen that for the maximum deformation 1.90, the areas of both the alpha and gamma component peaks decrease, so perhaps the material reaches its maximum orientation and the resulting strengthening between 1.56 and 1.90, while at deformation 1.90, the structure undergoes degradation, e.g., chain breakage, or other deformation if we assume that this is possible, or reorientation, deviations from this direction.

In the across direction:

- With an increase in deformation, the contribution of alpha components decreases, which seems logical because we deform the structure in the perpendicular direction and in the transverse direction, possibly occurring longitudinal chains of the alpha structure are deflected and deformed;
- For deformations 0.68, 1.25 and 1.56, the contribution of the gamma component increases systematically (reaching 100% of the contribution for deformation 1.56—there are no alpha components here);
- For deformation 1.90, we have the alpha component.1 but note that its surface area is absolutely marginal (0.06 is the level of 2% in the crystalline components and below 0.5% in the entire structure of the material taking into account the amorphous phase);
- What is more interesting is that for the 1.90 deformation, just as it was in the longitudinal direction for the alpha component, the surface of the gamma component also decreases, so the conclusion is similar to the above: the 1.90 deformation escapes from some of the systematics observed for the 0.68–1.56 range, and the structure changes in a less controlled and predictable way.

The HE process results in a clear increase in phase α participation to PA6. In the study by Peppin [21], it has been shown that in PA6, there is a transition $\gamma \rightarrow \alpha$ caused by mechanical impacts regardless of the temperature at which the deformation process took place, and Murthy [54], in the process of studying the PA6 γ fibers uniaxially drawn, observed transition from phase γ to a metastable structure.

3.4. Spectroscopy Analysis Results

The FTIR spectra of the tested PA6 before and after HE was analyzed, with example spectra, are shown in Figure 8. There were no significant shifts observed in the positions of the bands in the spectra of the samples, but there was a change in their intensity. Differences in the band intensities are also noted for the bands associated with the crystalline phase of the variety α : 1200, cm^{-1} , 1029, 960 and 929 cm^{-1} [38].

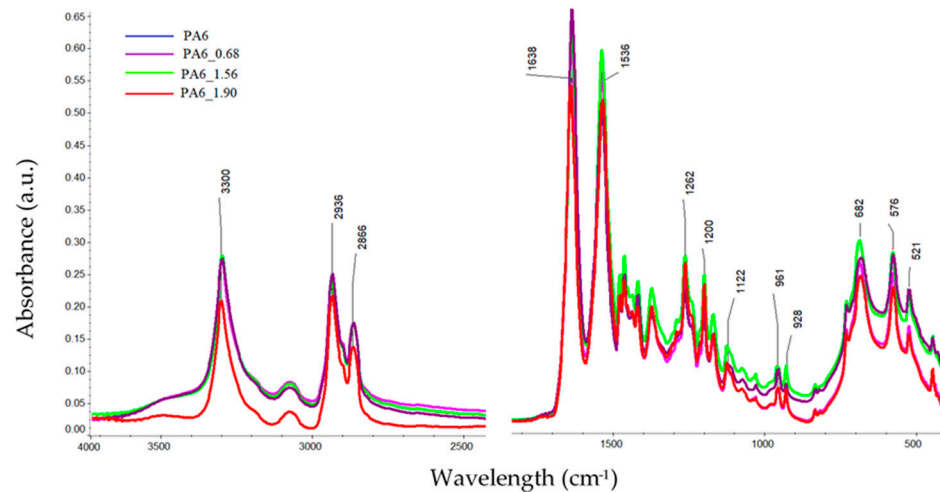


Figure 8. FTIR spectra of PA6 before and after the HE process at variable deformation.

To analyze the content of different forms of crystalline phases in PA6 samples before and after the HE process, fragments of spectra were analyzed for ranges typical of the PA6 crystal phase, i.e., $1200\text{--}900 \text{ cm}^{-1}$ [38]. The comparison was made for spectra collected from the center of cross-sections of samples made along the HE direction (Figure 9).

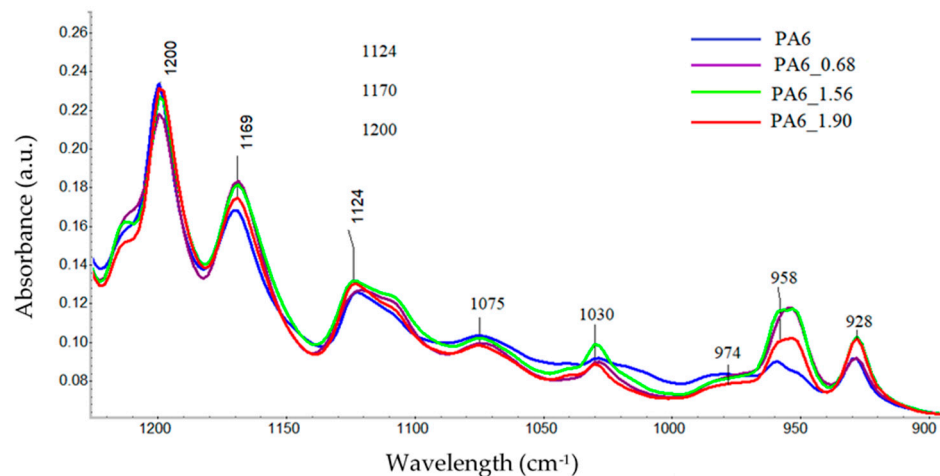


Figure 9. The spectral range typical of the crystalline phase in PA6 before and after the HE process.

Crystallinity indices of different varieties of crystallographic PA6 samples before and after the HE process at different deformations determined on the basis of FTIR are presented in Figure 10.

The nature of the changes in the crystallinity index of individual crystalline varieties α and γ determined on the basis of the FTIR analysis confirms the observations from the WAXS analysis that in the case of the PA6_1.56 sample, in the cross-section made along the HE direction, most of the crystalline phase takes the form of α . This result indicates a much higher orientation of the structural elements and a higher degree of ordering of the PA6_1.56 sample compared to other materials.

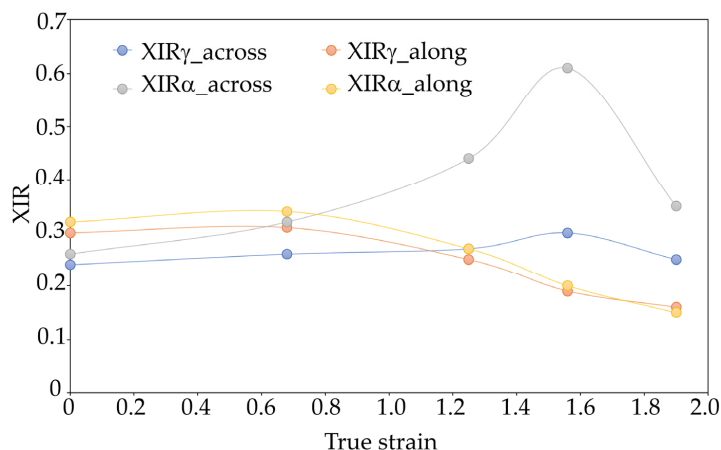


Figure 10. Crystallinity indices of various varieties of crystallographic PA6 samples before and after the HE process at different deformations determined on the basis of FTIR. Results of the FTIR analysis of the central part of the cross-section of the samples (across) and the cross-section made along the HE direction (along).

3.5. Results of Thermal Analysis Using Differential Scanning Calorimetry

Figures 11 and 12 show a comparison of selected DSC PA6 thermograms before and after the HE process at different deformations, taken from the central part of the rod.

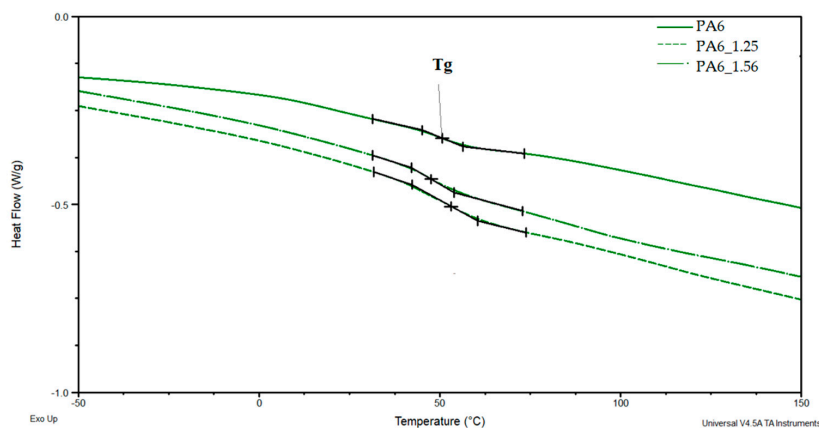


Figure 11. DSC PA6 thermograms before and after the HE process at different deformations in the range of glass transition temperature— T_g .

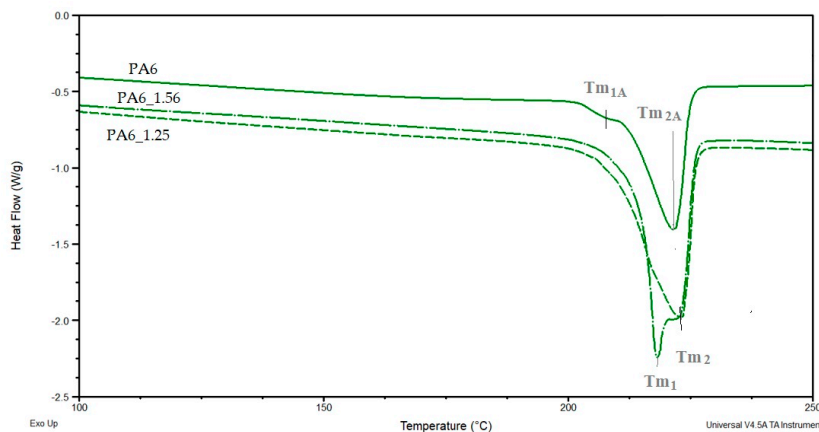


Figure 12. DSC PA6 thermograms before and after the HE process at different deformations in the melting point range— T_m .

Based on the DSC thermograms (Figures 11 and 12), the temperatures of glass transition T_{gA} and crystalline phase melting (T_{m1} and T_{m2}) of the PA6 were determined before and after the HE process leading to different sample deformations. The results of the distribution of the multiplet peaks associated with the crystalline phase melting are summarized in Figure 13.

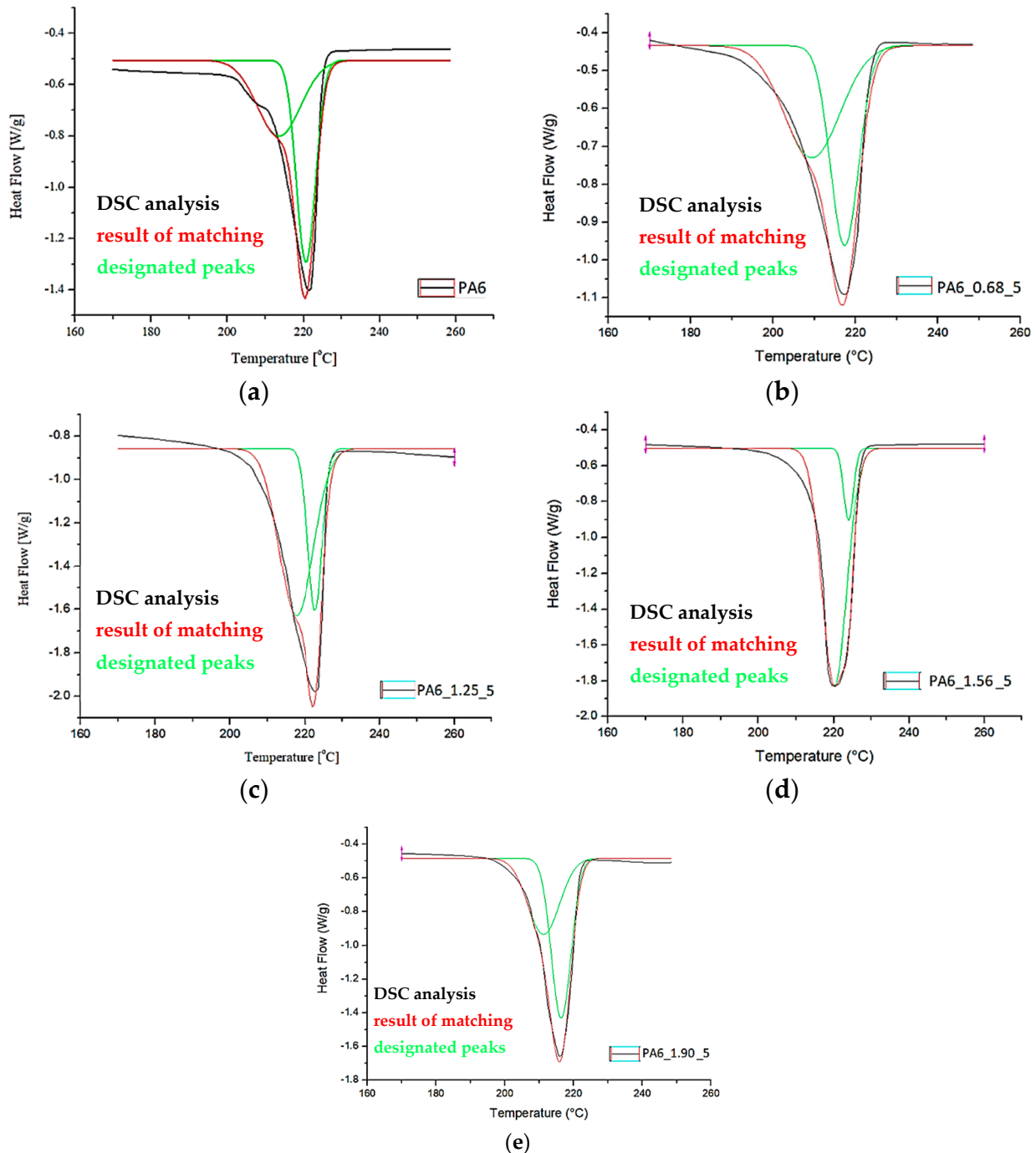


Figure 13. Distribution of the multiplet band from the melting of PA6 crystalline phase before (a) and after the HE process (b–e).

The melting enthalpy was also determined for each of the peaks that make up the multiplet peak associated with the crystalline phase melting. The results of the DSC analysis and the distribution of the crystal phase melting-related multiplet peaks are summarized in Table 4.

Table 4. Results of DSC analysis of PA6 samples before and after the HE process at different deformations of the samples taken from the middle part.

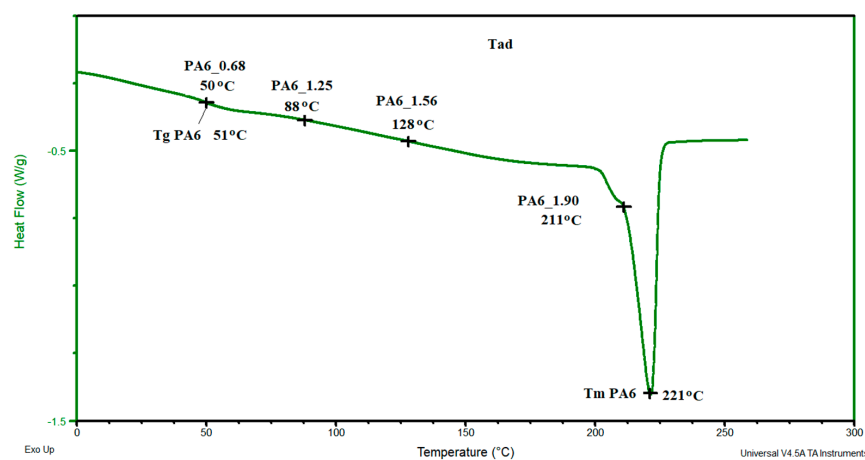
Series	T_g [°C]	T_{m1} [°C]	Peak Area— γ	T_{m2} [°C]	Peak Area— α	ΔH_m [J/g]	XDSC [%]
PA6	50.6 ± 1.2	214 ± 2	4.2 ± 0.2	221 ± 2	4.9 ± 0.1	58.3 ± 0.9	25.3
PA6_0.68	44.2 ± 1.1	209 ± 2	5.0 ± 0.3	217 ± 3	4.5 ± 0.2	71.3 ± 2.4	31.0
PA6_1.25	53.2 ± 0.6	218 ± 1	8.8 ± 0.5	223 ± 2	3.6 ± 0.1	78.4 ± 1.9	34.1
PA6_1.56	53.2 ± 0.4	220 ± 2	10.9 ± 0.7	224 ± 2	1.3 ± 0.1	85.0 ± 2.5	37.0
PA6_1.90	53.5 ± 0.3	211 ± 1	5.2 ± 0.2	216 ± 2	6.8 ± 0.3	71.9 ± 1.7	31.3

The glass transition temperature of PA6 is ca. 50.6 °C, reduced for the sample after the HE process at a small deformation of 0.68 (PA6_0.68) to ca. 44.2 °C. For other samples, T_g is ca. 53.2–53.5 °C. Changes in the microstructure of PA6 samples after the HE process cause slight differences in the mobility of the macromolecules of this polymer.

A multiplet endothermic peak with a melting point of the crystalline phase was observed in the PA6 sample at T_{m1} = ca. 214 °C and T_{m2} = ca. 221 °C. The first temperature can be associated with the melting of the crystalline phase of the variety γ which is usually ca. 214 °C [39], the second temperature T_{m2} for PA6 according to Millot et al. [15] is associated with phase α .

In samples PA6_0.68 and PA6_1.90, temperatures T_{m1} and T_{m2} are ca. 210 °C and ca. 217 °C. Both temperatures are lower than the melting points associated with the melting of phases γ and α . This indicates that these phases are defective.

In contrast, for samples PA6_1.25 and PA6_1.56, temperatures T_{m1} and T_{m2} are, respectively, ca. 219 °C and ca. 224 °C. The first of the temperatures can be associated with the melting of phase γ and the second with phase α . For these samples, the melting points of these phases are greater than the temperatures associated with their melting. Probably, as a result of the orientation of macromolecules in the HE process, more hydrogen bonds are formed between them, which contributes to an increase in the melting points of the individual phases. The results of the crystalline phase content calculations are summarized in Table 4. As the deformation increases in the HE process, the crystalline phase proportion increases, but for the 1.90 deformation, it is slightly less than for the 1.56 deformation. To explain the reason for the differences in the phase structure of PA6 after various deformations in the HE process, the change in adiabatic temperature generated during the HE process was analyzed (Figure 14).

**Figure 14.** DSC thermogram of PA6 sample with the applied adiabatic temperatures that were generated during the HE process of the tested samples.

In sample PA6_0.68, a temperature similar to that of PA6 was generated; in samples PA6_1.25 and PA6_1.56, respectively, temperatures of 88 and 128 °C were generated, and in

PA6_1.90, a temperature of 211 °C was generated. The adiabatic temperature for sample PA6_1.90 is greater than the initial melting point of the crystalline phase PA6. The change in the adiabatic temperature generated in PA6 during the HE process is an additional reason for the changes in the structure of the samples after the HE process. A similar phenomenon of changing the structure of PA6 samples but after the process of orientation and annealing at 200° was noted by Dencheeva et al. [54].

4. Conclusions

The HE process on the mechanical and structural properties of polyamides has not been systematically studied so far. Most of the tests carried out on other polymers were performed under conditions of increased temperature, especially in the process of conventional extrusion.

In this study, the structure of PA6 was analyzed after a hydrostatic extrusion process performed at a linear speed of 5 mm min⁻¹ and a variable deformation in the range of 0.68–1.90. As a result of the HE processes carried out at these parameters, a significant increase occurs in the strength properties determined in the static tensile test. The highest strength was obtained for samples after deformation of 1.56, and tensile strength rose by almost 500%.

As a result of microscopic observations using SEM, it was found that as a result of deformation in the HE process, the orientation of PA6 macromolecules along the deformation direction occurs.

POM images of cuttings of PA6 sample cross-sections confirmed the type of structure observed in the SEM images. As the true strain value rose, an increase was observed in the contribution of phase α in PA6 as a result of the analysis of WAXS. The results of the FTIR spectroscopic analysis confirm these observations that as the deformation increases, the proportion of the crystalline phase α rises. Thermal analysis using DSC allowed us to conclude that in the PA6 after the HE process generating deformations in the range of 0.68–1.56, the proportion of the crystalline phase α increases in PA6.

The observed changes in strength properties are due to the orientation of macromolecules and a slight increase in the proportion of the crystalline phase in these materials.

Author Contributions: Conceptualization, M.S. and J.R.; methodology, J.R., P.D. and M.S.; validation, J.R.; investigation, M.S., D.G., A.C., M.K. and P.D.; resources, M.S. and J.R.; writing—original draft preparation, M.S., M.K. and J.R.; writing—review and editing, M.S., M.K., J.R. and P.D.; visualization, M.S. and J.R. All authors have read and agreed to the published version of the manuscript.

Funding: This research received no external funding.

Institutional Review Board Statement: Not applicable.

Informed Consent Statement: Not applicable.

Data Availability Statement: The data presented in this study are available on request from the corresponding author.

Conflicts of Interest: The authors declare no conflict of interest.

References

1. Hill, R.G. Biomedical polymers. In *Biomaterials, Artificial Organs, and Tissue Engineering*; Woodhead Publishing Series in Biomaterials; Elsevier: Amsterdam, The Netherlands, 2005; pp. 97–106.
2. Richert, M.W.; Leszczynska-Madej, B.; Pachla, W.; Skiba, J. The Microstructure and Properties of Hydrostatically Extruded Polycrystalline Aluminium Al99.5. *Arch. Metall. Mater.* **2012**, *57*, 911–917. [[CrossRef](#)]
3. Kulczyk, M.; Przybysz, S.; Skiba, J.; Pachla, W. Severe Plastic Deformation Induced in Al, Al-Si, Ag and Cu by Hydrostatic Extrusion. *Arch. Metall. Mater.* **2014**, *59*, 59–64. [[CrossRef](#)]
4. Pachla, W.; Kulczyk, M.; Smalc-Koziorowska, J.; Przybysz, S.; Wróblewska, M.; Skiba, J.; Przybysz, M. Enhanced strength and toughness in ultra-fine grained 99.9% copper obtained by cryo-hydrostatic extrusion. *Mater. Charact.* **2018**, *141*, 375–387. [[CrossRef](#)]

5. Pachla, W.; Kulczyk, M.; Sus-Ryszkowska, M.; Mazur, A.; Kurzydowski, K.J. Nanocrystalline titanium produced by hydrostatic extrusion. *J. Mater. Process. Technol.* **2008**, *205*, 173–182. [[CrossRef](#)]
6. Pachla, W.; Skiba, J.; Kulczyk, M.; Przybysz, S.; Przybysz, M.; Wróblewska, M.; Diduszko, R.; Stępnia, R.; Bajorek, J.; Radomski, M.A.; et al. Nanostructuring of 316L type austenitic stainless steels by hydrostatic extrusion. *Mater. Sci. Eng. A-Struct. Mater. Prop. Microstruct. Process.* **2014**, *615*, 116–127. [[CrossRef](#)]
7. Skiba, J.; Pachla, W.; Mazur, A.; Przybysz, S.; Kulczyk, M.; Przybysz, M.; Wróblewska, M. Press for hydrostatic extrusion with back-pressure and the properties of thus extruded materials. *J. Mater. Process. Technol.* **2014**, *214*, 67–74. [[CrossRef](#)]
8. Pugh, H.L.D.; Low, A.H. The Hydrostatic Extrusion of Difficult Metals. *J. Inst. Met.* **1965**, *93*, 201–217.
9. Inoue, N.; Nakayama, T.; Shimono, M. Deformation of Polymers During Hydrostatic Extrusion. *J. Press. Vessel. Technol.* **1978**, *100*, 400–405. [[CrossRef](#)]
10. Inoue, N. *Hydrostatic Extrusion Theory and Applications*; Inoue, N., Nishihara, M., Eds.; Elsevier Applied Science Publishers: London, UK; New York, NY, USA, 1985; pp. 333–362.
11. Skorupska, M.; Kulczyk, M.; Przybysz, S.; Skiba, J.; Mizeracki, J.; Ryszkowska, J. Mechanical Reinforcement of Polyamide 6 by Cold Hydrostatic Extrusion. *Materials* **2021**, *14*, 6045. [[CrossRef](#)]
12. Wu, C.; Wu, R.; Xia, W.; Tam, L.-H. Understanding Creep Behavior of Semicrystalline Polymer via Coarse-Grained Modeling. *J. Polym. Sci. Part B Polym. Phys.* **2019**, *57*, 1779–1791. [[CrossRef](#)]
13. Li, Y.; Goddard, W.A., III. Nylon 6 Crystal Structures, Folds, and Lamellae from Theory. *Macromolecules* **2002**, *35*, 8440–8455. [[CrossRef](#)]
14. Zheng, J.; Siegel, R.W.; Toney, C.G. Polymer Crystalline Structure and Morphology Changes in Nylon-6/ZnO Nanocomposites. *J. Polym. Sci. Polym. Phys.* **2003**, *41*, 1033–1050. [[CrossRef](#)]
15. Millot, C.; Fillot, L.-A.; Lame, O.; Sotta, P.; Seguela, R. Assessment of polyamide-6 crystallinity by DSC Temperature dependence of the melting enthalpy. *J. Therm. Anal. Calorim.* **2015**, *122*, 307–314. [[CrossRef](#)]
16. Zhou, Q.; Fang, J.; Gao, H.; Loo, L.S. Substrate effects on the surface properties of nylon 6. *Appl. Surf. Sci.* **2013**, *282*, 115–120. [[CrossRef](#)]
17. Holmes, D.R.; Bunn, C.W.; Smith, D.J. The crystal structure of polycapromide: Nylon 6. *J. Polym. Sci.* **1955**, *17*, 159. [[CrossRef](#)]
18. Arimoto, H.; Ishibashi, M.; Hirai, M.; Chatani, Y. Crystal Structure of the γ -Form of Nylon 6. *J. Polym. Sci. A* **1965**, *3*, 317–326. [[CrossRef](#)]
19. Malta, V.; Cojazzi, G.; Fichera, A.; Ajo, D.; Zanetti, R. A re-examination of the crystal structure and molecular packing of α -nylon 6. *Eur. Polym. J.* **1979**, *15*, 765–770. [[CrossRef](#)]
20. Salem, D.R.; Weigmann, H.-D. Further discussion of the crystal structures of nylon 6. *Polym. Commun.* **1989**, *30*, 336.
21. Murthy, N.S. Metastable crystalline phases in nylon 6. *Polym. Commun.* **1991**, *32*, 301–305.
22. Abu-Isa, I. α - γ transition in nylon 6. *J. Polym. Sci. Polym. Chem. Edn.* **1971**, *9*, 199–216. [[CrossRef](#)]
23. Murthy, N.S.; Szollosi, A.B.; Sibilia, J.P.; Krimm, S. Stability of the γ form and the development of the α form in nylon 6. *J. Polym. Sci. Polym. Phys. Edn.* **1985**, *23*, 2549–2565. [[CrossRef](#)]
24. Miyasaka, K.; Makishima, K. Transition of Nylon 6. γ -Phase Crystals by Stretching in the Chain Direction. *J. Polym. Sci. Part A-1 Polym. Chem.* **1967**, *5*, 3017–3027.
25. Miyasaka, K.; Ishikawa, J. Effects of temperature and water on the $\gamma \rightarrow \alpha$ crystalline transition of nylon 6 caused by stretching in the chain direction. *J. Polym. Sci. Part A-2 Polym. Phys.* **1968**, *6*, 1317–1329. [[CrossRef](#)]
26. Hiramatsu, N.; Hirakawa, S. Melting and Transformation Behavior of γ Form Nylon 6 under High Pressure. *Polym. J.* **1982**, *14*, 165–171. [[CrossRef](#)]
27. Ziabicki, A. Derivate des Carbazols II. Die Darstellung von 3,6-Dihalogencarbazolen und ihre Nitrierung. *Collect. Czech. Chem. Commun.* **1957**, *22*, 64–75.
28. Ziabicki, A.; Kolloid, Z. Über die mesomorphe β -Form von Polycapronamid und ihre Umwandlung in die kristalline form α . *Colloid Polym. Sci.* **1959**, *167*, 132–141. [[CrossRef](#)]
29. Ziabicki, A.; Kedzierska, K. Studies on the orientation phenomena by fiber formation from polymer melts. Part I. Preliminary investigations on polycapronamide. *J. Polym. Sci.* **1959**, *2*, 14–23. [[CrossRef](#)]
30. Avramova, N.; Fakirov, S. The β -structure of nylon-6 determined by reflection high energy electron diffraction. *Polym. Commun.* **1984**, *25*, 27–29.
31. Roldan, L.G.; Kaufman, H.S. Crystallization of nylon 6. *Polym. Lett.* **1963**, *1*, 603–608. [[CrossRef](#)]
32. Illers, K.H.; Haberkorn, H.; Simak, P. Untersuchungen über die γ -struktur in unverstrecktem und verstrecktem 6-polyamid. *Makromol. Chem.* **1972**, *158*, 285–311. [[CrossRef](#)]
33. Stepaniak, R.F.; Garton, A.; Carlsson, D.J.; Wiles, D.M.J. An examination of the crystal structures present in nylon-6 fibers. *Polym. Sci. Polym. Phys. Ed.* **1979**, *17*, 987–999. [[CrossRef](#)]
34. Startsev, O.V.; Iordanskii, A.L.; Zaikov, G.Y. Effect of the $\gamma^* \rightarrow \alpha$ -structural transition, occurring in the presence of mineral acids, on the molecular mobility and relaxation processes in polyamide-6. *Polym. Sci. USSR* **1988**, *30*, 1625–1631. [[CrossRef](#)]
35. Auriemma, F.; Petraccone, V.; Parravicini, L.; Corradini, P. Mesomorphic form (β) of nylon 6. *Macromolecules* **1997**, *30*, 7554–7559. [[CrossRef](#)]
36. Wunderlich, B. *Macromolecular Physics, Volume 3: Crystal Melting*; Academic Press: New York, NY, USA, 1980.
37. Megatech. Available online: <https://megatech24.eu/> (accessed on 28 July 2022).

38. Dechant, J. *Ultraspektroskopische Untersuchungen an Polymeren*; Akademie-Verlag: Berlin, Germany, 1972.
39. Osorio, D.A.; Niinivaara, E.; Jankovic, N.C.; Demir, E.C.; Benkaddour, A.; Jarvis, V.; Ayranci, C.; McDermott, M.T.; de Lannoy, C.-F.; Cranston, E.D. Cellulose Nanocrystals Influence Polyamide 6 Crystal Structure, Spherulite Uniformity, and Mechanical Performance of Nanocomposite Films. *Appl. Polym. Mater.* **2021**, *3*, 4673–4684. [[CrossRef](#)]
40. Pawlak, A.; Galeski, A. Plastic Deformation of Crystalline Polymers: The Role of Cavitation and Crystal Plasticity. *Macromolecules* **2005**, *38*, 9688–9697. [[CrossRef](#)]
41. Bartczak, Z.; Galeski, A. Yield and plastic resistance of α -crystals of isotactic polypropylene. *Polymer* **1999**, *40*, 3677–3684. [[CrossRef](#)]
42. Haudin, J.M. *Plastic Deformation of Amorphous and Semicrystalline Materials*; Escaig, B., G'Sell, C., Eds.; Les Editions de Physique: Paris, France, 1982; p. 291.
43. Alcock, B. *Single Polymer Composites Based on Polypropylene: Processing and Properties*; Materials Department, Queen Mary University of London: London, UK, 2004.
44. Fu, D.; Kuang, T.; Chen, F.; Lee, L.J.; Peng, X. Fabrication of high strength PA6/PP blends with pressure-induced flow Processing. *Mater. Chem. Phys.* **2015**, *164*, 1–5. [[CrossRef](#)]
45. Kohan, M. *Nylon Plastics Handbook*; Hanser/Gardner Publications, Inc.: Cincinnati, OH, USA, 1995.
46. Ito, M.; Mizuochi, K.; Kanamoto, T. Effects of crystalline forms on the deformation behaviour of nylon-6. *Polymer* **1998**, *39*, 4593–4598. [[CrossRef](#)]
47. Chae, D.W.; Oh, S.G.; Kim, B.C. Effect of Silver Nanoparticles on the Dynamic Crystallization Behavior of Nylon-6. *J. Polym. Sci. Polym. Phys.* **2004**, *42*, 790–799. [[CrossRef](#)]
48. Fornes, T.D.; Paul, D.R. Crystallization Behavior of Nylon 6 Nanocomposites. *Polymer* **2003**, *44*, 3945–3956. [[CrossRef](#)]
49. Murase, S.; Inou, A.; Miyashita, Y.; Kimura, N.; Nishio, Y. Structural Characteristics and Moisture Sorption Behavior of Nylon-6/Clay Hybrid Films. *J. Polym. Sci. Polym. Phys.* **2002**, *40*, 479–487. [[CrossRef](#)]
50. Wu, Q.; Liu, X.; Berglund, L.A. FT-IR Spectroscopic Study of Hydrogen Bonding in PA6/Clay Nanocomposites. *Polymer* **2002**, *43*, 2445–2449. [[CrossRef](#)]
51. Dai, R.; Huang, M.; Ma, L.; Liu, W.; He, S.; Liu, H.; Zhu, C.; Wang, Y.; Zhang, Z.; Sun, A. Study on crystal structure and phase transitions of polyamide 12 via wide-angle X-ray diffraction with variable temperature. *Adv. Compos. Hybrid Mater.* **2020**, *3*, 522–529. [[CrossRef](#)]
52. Liu, Y.; Cui, L.; Guan, F.; Gao, Y.; Hedin, N.E.; Zhu, L.; Fong, H. Crystalline Morphology and Polymorphic Phase Transitions in Electrospun Nylon 6 Nanofibers. *Macromolecules* **2007**, *40*, 6283–6290. [[CrossRef](#)]
53. Pepin, J.; Gaucher, V.; Rochas, C.; Lefebvre, J.-M. In-situ SAXS/WAXS investigations of the mechanically-induced phase transitions in semi-crystalline polyamides. *Polymer* **2019**, *175*, 87–98. [[CrossRef](#)]
54. Dencheva, N.; Denchev, Z.; Oliveira, M.J.; Funari, S.S. Relationship between crystalline structure and mechanical behavior in isotropic and oriented polyamide 6. *J. Appl. Polym. Sci.* **2007**, *103*, 2242–2252. [[CrossRef](#)]

Disclaimer/Publisher's Note: The statements, opinions and data contained in all publications are solely those of the individual author(s) and contributor(s) and not of MDPI and/or the editor(s). MDPI and/or the editor(s) disclaim responsibility for any injury to people or property resulting from any ideas, methods, instructions or products referred to in the content.